Journal of Medicinal Chemistry

Article

pubs.acs.org/jmc

New 5-Unsubstituted Dihydropyridines with Improved $Ca_V1.3$ Selectivity as Potential Neuroprotective Agents against Ischemic Injury

Giammarco Tenti,[†,#] Esther Parada,[‡,#] Rafael León,[*,‡,§] Javier Egea,[‡] Sonia Martínez-Revelles,[∥] Ana María Briones,[∥] Vellaisamy Sridharan,[†,⊥] Manuela G. López,[‡,§,∥] María Teresa Ramos,[†] and J. Carlos Menéndez[*,†]

[†]Departamento de Química Orgánica y Farmacéutica, Facultad de Farmacia, Universidad Complutense, 28040 Madrid, Spain

[‡]Instituto Teófilo Hernando y Departamento de Farmacología y Terapéutica, Facultad de Medicina, Universidad Autónoma de Madrid, 28029 Madrid, Spain

[§]Instituto de Investigación Sanitaria, Servicio de Farmacología Clínica, Hospital Universitario de la Princesa, 28006 Madrid, Spain

[∥]Departamento de Farmacología y Terapéutica, Facultad de Medicina, Universidad Autónoma de Madrid, Instituto de Investigación del Hospital Universitario La Paz (IdiPAZ), 28029 Madrid, Spain

[⊥]Department of Chemistry, School of Chemical and Biotechnology, SASTRA University, Thanjavur 613401, Tamil Nadu, India

Supporting Information

ABSTRACT: C_5-unsubstituted-C_6-aryl-1,4-dihydropyridines were prepared by a CAN-catalyzed multicomponent reaction from chalcones, β-dicarbonyl compounds, and ammonium acetate. These compounds were able to block Ca^{2+} entry after a depolarizing stimulus and showed an improved $Ca_v1.3$/$Ca_v1.2$ selectivity in comparison with nifedipine. Furthermore, they were able to protect neuroblastoma cells against Ca^{2+} overload and oxidative stress models. Their selectivity ratio makes them highly interesting for the treatment of neurological disorders where Ca^{2+} dyshomeostasis and high levels of oxidative stress have been demonstrated. Furthermore, their low potency toward the cardiovascular channel subtype makes them safer by reducing their probable side effects, in comparison to classical 1,4-dihydropyridines. Some compounds afforded good protective profile in a postincubation model that simulates the real clinical situation of ictus patients, offering a therapeutic window of opportunity of great interest for patient recovery after a brain ischemic episode. Good activities were also found in acute ischemia/reperfusion models of oxygen and glucose deprivation.

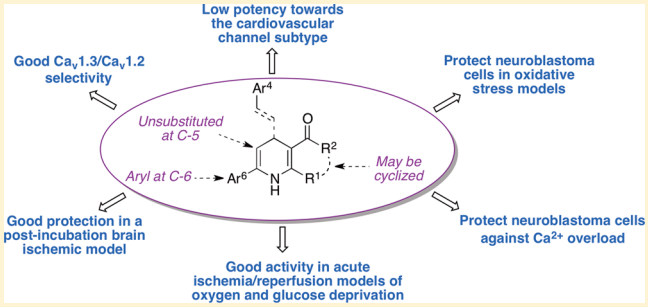

INTRODUCTION

Neurodegenerative disorders constitute a significant public health problem worldwide, and among these, cerebrovascular accidents represent one of the leading causes of death, neurological disability, and cognitive impairment.[1] In the past years, significant progress has been made in the understanding of the physiopathology of stroke, leading to the description of several pathological features that are common with other neurodegenerative disorders. These features include protein misfolding and aggregation, excitotoxicity, oxidative stress, and an ionic imbalance (especially with reference to Ca^{2+}), which is associated with mitochondrial dysfunction.[2] These concepts are the basis for the development of molecules that could be employed as neuroprotective agents, a long-standing objective of modern medicine.[3] During cerebral ischemia, oxygen and glucose deprivation induces a metabolic cascade that leads to neuronal death. One of the most significant consequences of these changes is the dysregulation of Ca^{2+} homeostasis, leading to brain damage. In this context, the stabilization of Ca^{2+} homeostasis by blocking neuronal voltage-gated calcium channels (VGCCs) could represent one important approach for postischemic neuroprotection in humans.[4]

VGCCs are multimeric membrane proteins that play a critical role in many physiological functions in a variety of tissues.[5] These proteins are usually classified into three broad groups (Ca_V1, Ca_V2, and Ca_V3) and different subtypes depending on the pore-forming subunit. The members of the Ca_V1 family represent the most intensely studied channels and are classified in four diverse isoforms ($Ca_V1.1$−$Ca_V1.4$) that differ in their tissue distributions and physiological functions.[6] $Ca_V1.2$ VGCCs are the major and most targeted isoform,[7] found mainly in the cardiovascular system, where they control vascular tone, although they are also found in neurons. $Ca_V1.3$ VGCCs have a tissue distribution similar to that of

Received: February 18, 2014
Published: April 22, 2014

   dx.doi.org/10.1021/jm500263v | J. Med. Chem. 2014, 57, 4313−4323

$Ca_V1.2$ VGCCs, but they are more neurospecific and are believed to have an important role in neuronal excitability.[8]

Recent studies[9] have demonstrated the implication of Ca^{2+} entry through $Ca_V1.3$ VGCCs in the generation of oxidative stress underlying the pathogenesis of Parkinson's disease. Therefore, selective antagonism of $Ca_V1.3$ VGCCs is considered a potential neuroprotective strategy that could slow neuronal loss in the early stages of Parkinson's disease.[10] Among VGCCs blockers, 1,4-dihydropyridines (DHPs) can certainly be considered the most extensively studied family because of their pharmacological versatility.[11] It is known that high doses of DHPs, such as nifedipine, induce some beneficial brain effects such as amelioration of age-related working memory deficits among others.[12] Indeed, nifedipine binds both $Ca_V1.2$ and $Ca_V1.3$ isoforms, although it shows high selectivity toward $Ca_V1.2$, a characteristic that is a key requirement for its use in cardiovascular therapy, but that, coupled to its difficulty in crossing the blood–brain barrier, prevents its use as a neuroprotective agent.[12] Therefore, a major drawback that needs to be addressed in this area is the prevalence of vascular side effects of currently used DHPs. Thus, a renewed interest exists on the search and study of selective $Ca_V1.3$ L-type VGCCs in the context of efforts to find $Ca_V1.3$ L-type VGCC-selective protective agents for neurodegenerative diseases (NDDs).[10,13]

Against this background, we have recently reported, in preliminary fashion,[14] the synthesis and initial pharmacological evaluation of a small library of DHP derivatives able to prevent neuronal $[Ca^{2+}]_c$ overload by blockade of L-type VGCCs and neuroprotective effect against oxidative stress in vitro. In this work, we now report the extension of the initial library of compounds and a full pharmacological characterization in order to achieve a better understanding of their structure–activity relationships (SARs). We have evaluated the ability of our DHPs to antagonize selectively $Ca_V1.3$ VGCCs, with a view to contribute to the search for new neuroprotective agents for the treatment of NDDs and cerebral ischemia. We have also extended the investigation of their biological activity by using pharmacological assays that reproduce the pathological conditions of an ischemic episode. In all cases, the substitution pattern of these derivatives, especially the absence of a substituent at C-5 and the presence of an aryl group at C-6, was predicted to lead to a reduced vascular activity. It is pertinent to note here that the C-5 substituent is known to have an influence on the tissue selectivity of 1,4-dihydropyridines and also on the antagonistic/agonistic character of the DHPs (Figure 1).[15] Additional neuroprotective mechanisms have also been investigated.

RESULTS AND DISCUSSION

Chemistry. For the preparation of the dihydropyridine library, we employed a three-component reaction between β-dicarbonyl compounds **1**, chalcones **2**, and ammonium acetate as a source of ammonia in refluxing ethanol and in the presence of ceric ammonium nitrate (CAN) as a Lewis acid catalyst (Scheme 1).[16] This formal [3 + 3] aza-annulation took place presumably by a Hantzsch-like mechanism involving the initial formation of a β-enaminone from compound **1** and ammonia, followed by its Michael addition onto **2** and a final cyclocondensation with loss of a molecule of water. This mechanism was supported by performing the reaction between commercially available ethyl 3-aminocrotonate and chalcone,

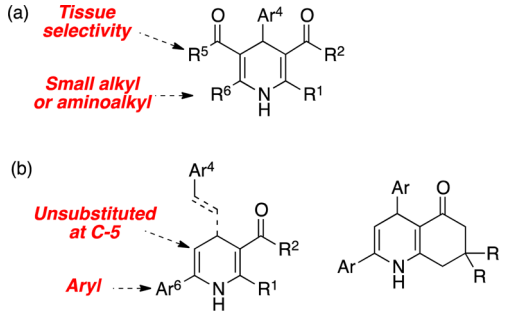

Figure 1. Comparison between traditional 1,4-dihydropyridines with cardiovascular activity (a) and the compounds studied in this paper (b).

Scheme 1

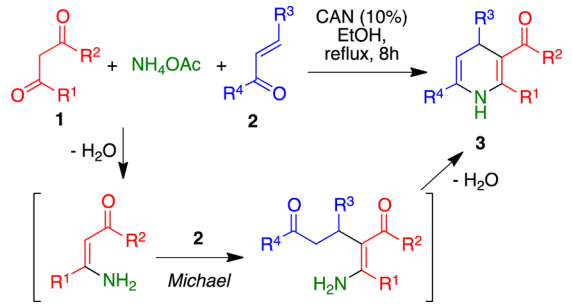

which afforded compound **3a** under the same conditions employed for the multicomponent reaction.

This method allowed the preparation of good to excellent yields of the compounds summarized in Table 1, bearing small alkyl groups at C-2, ester, thioester, or ketone groups at C-3, a variety of aryl, heteroaryl, or styryl substituents at C-4, no substitution at C-5, and aryl or heteroaryl groups at C-6.

In order to explore the influence of a higher rigidity on the activity and selectivity of our compounds, we also prepared

Table 1. Scope and Yields of the DHP Synthesis

compd	R^1	R^2	R^3	R^4	yield, %
3a[17]	CH_3	OEt	C_6H_5	C_6H_5	95
3b[14]	C_2H_5	OEt	C_6H_5	C_6H_5	92
3c	C_3H_7	OEt	C_6H_5	C_6H_5	81
3d[14]	CH_3	S^{t}Bu	C_6H_5	C_6H_5	99
3e[18]	CH_3	CH_3	C_6H_5	C_6H_5	56
3f[17]	CH_3	OEt	C_6H_5	4-ClC_6H_4	71
3g	CH_3	OEt	4-ClC_6H_4	4-ClC_6H_4	86
3h[17]	CH_3	OEt	4-$MeOC_6H_4$	C_6H_5	73
3i[14]	CH_3	S^{t}Bu	4-$MeOC_6H_4$	C_6H_5	69
3j	CH_3	OEt	3-$MeOC_6H_4$	4-ClC_6H_4	75
3k[14]	CH_3	S^{t}Bu	4-BrC_6H_4	4-MeC_6H_4	67
3l[14]	CH_3	S^{t}Bu	4-MeC_6H_4	C_6H_5	99
3m[14]	CH_3	S^{t}Bu	4-MeC_6H_4	4-MeC_6H_4	97
3n[17]	CH_3	OEt	4-MeC_6H_4	C_6H_5	94
3o	CH_3	OAllyl	C_6H_5	4-ClC_6H_4	78
3p[19]	CH_3	OEt	4-$NO_2C_6H_4$	C_6H_5	96
3q	CH_3	OEt	2-$NO_2C_6H_4$	4-MeC_6H_4	78
3r	CH_3	OEt	2-$NO_2C_6H_4$	4-ClC_6H_4	62
3s[14]	CH_3	OEt	2-Thienyl	4-MeC_6H_4	57
3t	CH_3	OEt	4-MeC_6H_4	2-Furyl	49
3u[14]	CH_3	S^{t}Bu	C_6H_5-CH=C(CH_3)	C_6H_5	52

dx.doi.org/10.1021/jm500263v | J. Med. Chem. 2014, 57, 4313–4323

hexahydroquinolines **5** by application of the CAN-catalyzed multicomponent protocol to 1,3-cyclohexanedione and dimedone (Scheme 2).[20]

Scheme 2

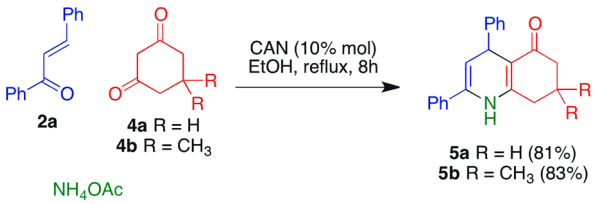

Pharmacology. *Neuronal VGCC Blockade in SH-SY5Y Neuroblastoma Cells.* As previously mentioned, DHPs are specific L-type VGCC blockers. Their activity and vascular selectivity require an ester functionality at C-5 and a small alkyl or aminoalkyl substituent at C-6.[15] According to our preliminary data, some compounds **3** blocked the $[Ca^{2+}]_c$ elevation elicited by 70 mM K^+ in the neuronal type cells.[14] IC_{50} values for Ca^{2+} signal blockade data of newly obtained DHPs are collected in Table 2, using nifedipine as the reference drug. Most DHPs showed moderate to high potency to block neuronal L-type VGCCs, with IC_{50} values ranging from more than 100 μM (compound **3m**) to 2.8 μM (compound **5b**).

Table 2. IC_{50} Values of Compounds 3a−u and 5a,b Calculated as Blockade of $[Ca^{2+}]_c$ Increase Elicited by 70 mM K^+ in SH-SY5Y Cells

compd	IC_{50} (μM)[a]
nifedipine	1.35 ± 0.4
3a	18.7 ± 6.6
3b[14]	12.8 ± 2.1
3c	9.9 ± 2.6
3d	95.8 ± 5.7
3e	27.1 ± 3.4
3f	9.3 ± 1.1
3g	28.4 ± 3.2
3h	29.8 ± 4.8
3i[14]	26.8 ± 3.7
3j	15.1 ± 2.8
3k	59.6 ± 9.1
3l	56.2 ± 6.4
3m	>100
3n	20.6 ± 2.1
3o	18.5 ± 1.1
3p	12.2 ± 1.4
3q	44.1 ± 8.2
3r	57.1 ± 6.6
3s	14.9 ± 3.8
3t	55.5 ± 5.4
3u	63.1 ± 3.0
5a	24.0 ± 6.4
5b	2.8 ± 0.8

[a]IC_{50} values were determined from dose−response curves (1−100 μM). Data are expressed as the mean ± SEM of three to six different cultures in triplicate.

Regarding SAR studies related to the ester functionality, ethyl ester derivatives were, in general, better VGCCs blockers than *tert*-butyl thioester derivatives. Thus, compound **3n** (ethyl ester and C-4 *p*-Me-phenyl) was 2.7 times more potent than **3l** (thioester and C4 *p*-Me-phenyl) and more than 4.8 times better than **3m** (thioester and C-6, C-4 *p*-Me-phenyl). The lower Ca^{2+} channel blocking properties of thioester derivatives might be related to an increased steric hindrance originated by the high volume of the *t*-Bu thioester group. As an exception, compound **3i**, a thioester derivative bearing a C-4 *p*-OMe-phenyl substituent, was slightly more potent than its parent ethyl ester derivative **3h**. On the other hand, compound **3m**, showing two *p*-Me-phenyl groups at C-4 and C-6, showed the lowest potency, with an IC_{50} value above 100 μM. Among ethyl ester derivatives, compound **3c** was the most potent with an IC_{50} value of 9.9 μM.

Regarding the effect of the substituents present at the dihydropyridine ring, replacement of the methyl group at C-2 (**3a**) by an ethyl (**3b**) or propyl group (**3c**) improved their blocking properties from 18.7 μM for compound **3a** to 12.8 μM for **3b** and 9.9 μM for **3c**. Bicyclic derivatives **5a** and **5b**, which can also be viewed as C-2 modified analogues of **3a**, showed good potencies, especially compound **5b**, which blocked the Ca^{2+} signal induced by high potassium levels with an IC_{50} of 2.8 μM, being the most potent VGCCs blocker of the series and almost as potent as nifedipine. Its analogue **5a**, which shares the same tetrahydroquinolin-5-(1*H*)-one core but lacks the two methyl substituents at position 7, was 8.6 times less potent than **5b**.

In terms of the substituents present at C-4 of the dihydropyridine ring, compounds bearing unsubstituted phenyl rings were generally better blockers than those having rings possessing electron-donating or electron-withdrawing groups.

Finally, comparing different substituents at position C-6, electron-withdrawing substituents derivatives were in general more potent VGCC blockers than the corresponding phenyl derivatives. Also generally speaking, derivatives bearing a *p*-Me-phenyl moiety were poorer blockers than phenyl derivatives.

Functional Assay: $Ca_V1.2$ and $Ca_V1.3$ IC_{50} Determination and Selectivity Comparison. As stated above, $Ca_V1.2$ L-type VGCCs are the major isoform (~90%),[21] expressed in cardiac myocytes, smooth muscle, and pancreas while $Ca_V1.3$ channels are more neuron-specific (cerebral cortex, hippocampus, basal ganglia, habenula, and thalamus) and are thought to serve predominantly as modulators in the neuronal system. $Ca_V1.3$ is connected to mitochondrial oxidative stress and increased vulnerability in SNc dopaminergic neurons.[9a,22]

Because of our goal of reducing cardiovascular effects in neuroprotective DHPs, it was crucial to study the $Ca_V1.3$/$Ca_V1.2$ L-type VGCCs selectivity of these C-5 unsubstituted DHPs. SH-SY5Y neuroblastoma cells were used to study the blockade of $Ca_V1.3$ L-type VGCCs.[23] Compounds **3n**, **3u**, and **5b** were selected to calculate their IC_{50} values for $Ca_V1.3$ L-type VGCCs because of their Ca^{2+} blockade properties and their overall neuroprotective profile (see Tables 4 and 5). Compound **5b** showed the best IC_{50} to block Ca^{2+} entry through neuronal L-type VGCCs (IC_{50} = 2.81 μM) displaying only half potency of that calculated for nifedipine (IC_{50} = 1.35 μM), a classical, highly potent L-type VGCCs blocker. Compounds **3n** and **3u** were less potent, with IC_{50} values of 20.6 and 63.1 μM, respectively (Table 3).

To calculate the $Ca_V1.3$/$Ca_V1.2$ selectivity ratio, we used the relaxation induced by each compound in 70 mM K^+ precontracted rat mesenteric resistance arteries. All DHPs induced concentration-dependent relaxation responses. The relaxation induced by nifedipine was higher than that induced by **3n**, **3u**, and **5b** (Table 3). Nifedipine blocked the $Ca_V1.2$

dx.doi.org/10.1021/jm500263v | J. Med. Chem. 2014, 57, 4313−4323

Table 3. IC_{50} Values for VGCC Blockade by Nifedipine and Compounds 3n, 3u, and 5b

	exptl IC_{50} (μM)		
compd	neuronal (SH-SY5Y)	cardiovascular (70 mM K^+)	$Ca_V1.3/Ca_V1.2$
nifedipine	1.35	0.00142	950.7
3n	20.6	10.6	1.9
3u	63.1	20.3	3.1
5b	2.81	0.34	8.3

cardiovascular subtype more potently than neuronal channels by a factor of 950, showing a high selectivity for the $Ca_V1.2$ VGCC subtype. On the contrary, our modifications in the DHP structure have resulted in a drastic decrease in their selectivity toward $Ca_V1.2$ cardiovascular subtype (Table 3). Compound **5b**, the most potent VGCCs blocker of the new family, showed the highest selectivity toward $Ca_V1.2$ subtype, since it was 8.3 times more potent toward this subtype than for neuronal $Ca_V1.3$. Nevertheless, this result represents a $Ca_V1.3/Ca_V1.2$ selectivity more than 100 times lower than that of nifedipine. This reduction on selectivity was even higher for compounds **3u** and **3n**, which were 306- and 500-fold less selective toward $Ca_V1.2$ subtype than the reference compound. Similar results were obtained when U46619 was used as precontraction stimulus (data not shown). Thus, **3n** and **3u** have drastically improved their selectivity toward the $Ca_V1.3$ by lowering their potency toward the cardiovascular subtype while maintaining their activity in the neuronal subtype. The $Ca_V1.3/Ca_V1.2$ achieved by these compounds represents a substantial improvement even over isradipine, which so far was the DHP with the highest relative affinity for $Ca_V1.3$ L-type VGCCs but which is still $Ca_V1.2$-selective.[22]

Molecular Modeling. We performed docking calculations to acquire deeper insights into the molecular basis for the interaction of these new C5-unsubstituted DHPs with $Ca_V1.2$ L-type channels. Although the X-ray structure of the L-type VGCCs is not available, several models have been described in recent years, among which we have used the one developed by Zhorov et al.[24] We have maintained the nomenclature used by these authors for a better understanding. Experimental mutagenesis results[25] and predicted interactions[13b,24,26] have located the DHP binding site in the interface of domains III and IV of the pore-forming α_1 subunit, in transmembrane segments IIS5, IIIIS6, IVS6, and IIIP.

It is known that although potent DHP antagonists have H-bond acceptors at both the port and starboard sides and H-bond donors at the stern, elimination of the port side ester group does not abolish the channel-blocking effect of DHPs.[27] We performed our docking calculations with nifedipine as a reference compound. As shown in Figure 2A, nifedipine shares a similar position as that found for (*S*)-nimodipine, in which the NH group (stern) H-bonds to Y^{3i10}. Nifedipine also has a polar *o*-NO_2 group at the bowsprit that H-bonds to Y^{4i11} and this residue, in turn, H-bonds to the carboxymethyl ester moiety present at port side.

Then we docked compound **3n** using the previously optimized settings, constraining the calculations to the DHP binding region where, presumably, these new 5-unsubstituted DHPs may interact. We docked the (*S*)-**3n** enantiomer because it leaves the unsubstituted configuration at the port side position, and as we mentioned before, this deletion does not abolish the antagonistic activity by itself. The (*S*)-**3n** enantiomer presents a 2-methyl and ethyl 3-carboxylate groups at the starboard side and a bulky phenyl moiety at the port side, and more importantly, it lacks the second carboxylic ester functionality at the port side. Docking results of (*S*)-**3n** (Figure 2B) predict an orientation of the DHP core similar to that found for nifedipine but show a noticeably different interaction pattern. The inclusion of a bulky Ph group increases the steric hindrance with F^{3p49}, and therefore (*S*)-**3n** appears displaced toward the side entry of the DHP binding site formed by M^{3i18}, M^{4i12}, T^{3o16}, and S^{4i9} (not shown). Thus, the phenyl moiety at the port side is partially accommodated in a hydrophobic pocked formed by M^{3i19} and F^{3p49} and the core of DHP is slightly displaced away from the selectivity pore of the channel. The NH at the stern H-binds to Y^{3i10} and the carbonyl group at the starboard establishes an H-bond to Q^{3o18}.

Comparing both complexes, we can conclude that the absence of several H-bond interactions and the inclusion of a bulky group at port side are destabilizing the interaction between our 5-unsubstituted DHPs and the $Ca_V1.2$ L-type VGCCs. These results, together with our experimental data, give some hints of the reason for the observed decrease in selectivity toward $Ca_V1.2$.

Neuroprotection: $[Ca^{2+}]_c$ Overload Model. A tight control of Ca^{2+} homeostasis by neurons is crucial for cell survival. In several NDDs, Ca^{2+} dysregulation is thought to be one of the main causes of neurodegeneration.[28] Thus, drugs restoring the Ca^{2+} balance should indeed be a therapeutic alternative for the disease.[29]

In line with these findings, our preliminary study[14] showed an interesting neuroprotective profile of the C5-unsubstituted DHPs against $[Ca^{2+}]_c$ overload and oxidative stress. This study

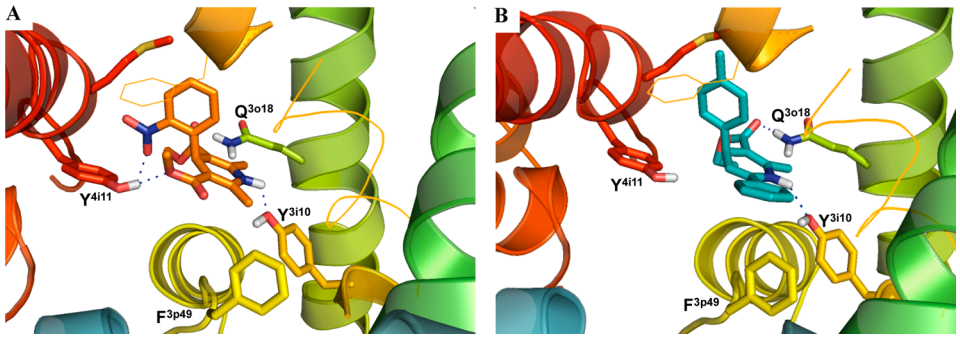

Figure 2. Docked structures of nifedipine (orange sticks, panel A) and compound **3n** (blue sticks, panel B) in the DHP binding site of the $Ca_V1.2$ L-type VGCC model. H-bond interactions are represented dashed blue lines. Key interacting residues are displayed in colors selected by chain.

dx.doi.org/10.1021/jm500263v | J. Med. Chem. 2014, 57, 4313−4323

was completed by investigating the potential neuroprotective activity of the novel compounds **3a**−**u** and **5a**,**b** on SH-SY5Y cells exposed for 24 h to a depolarizing concentration of K^+, which induced $[Ca^{2+}]_c$ overload and consequently cell death. Cells were co-incubated with drugs at 5 μM and high K^+ (70 mM, hypertonic). Thereafter, MTT reduction was measured as a parameter of cell death.[30] As shown in Table 4, newly

Table 4. Neuroprotection Exerted by Compounds 3a−u and 5a,b against Ca^{2+} Overload Induced by 70 mM K^+ in SH-SY5Y Human Neuroblastoma Cells[a]

	K^+ (70 mM co-incubation)	
compd	% survival	% protection
basal	100	
70 mM K^+	52.1 ± 3.5$^{###}$	
nifedipine (5 μM)	62.9 ± 3.4*	20.0
nifedipine (0.3 μM)	58.7 ± 2.2*	15.8
3a[14]	67.6 ± 3.1***	34.6
3b[14]	67.3 ± 2.3***	31.4
3c	65.4 ± 3.3*	23.3
3d[14]	68.0 ± 2.2***	34.1
3e[14]	67.4 ± 1.4***	32.5
3f[14]	69.4 ± 2.4***	36.6
3g	65.1 ± 4.2 *	24.8
3h	69.4 ± 3.6**	34.1
3i[14]	66.7 ± 2.9***	31.3
3j	72.7 ± 2.9***	40.1
3k[14]	67.2 ± 3.3***	34.5
3l[14]	67.4 ± 1.9***	30.4
3m[14]	69.9 ± 2.4***	36.2
3n	72.3 ± 3.6***	39.8
3o	68.7 ± 2.5***	29.8
3p	64.6 ± 4.3*	23.5
3q	62.9 ± 5.7*	22.1
3r	59.3 ± 5.5^{ns}	13.7
3s[14]	75.6 ± 2.1***	50.7
3t	68.5 ± 3.7**	32.0
3u[14]	69.0 ± 2.6***	35.3
5a[14]	66.4 ± 1.3***	28.2
5b	64.0 ± 4.1*	21.4

[a]Data are the mean ± SEM of at least five different cultures in triplicate. % protection was calculated considering MTT reduction by nontreated cells (basal) as 100% survival. % of toxicity was normalized for 70 mM K^+ seen for each treatment and subtracted to 100. (***) $p < 0.001$. (**) $p < 0.01$. (*) $p < 0.05$. ns = not significant with respect to 70 mM K^+ treated cells. (###) $p < 0.001$ compared to basal conditions. All compounds were assayed at 5 μM.

obtained DHPs showed a similar profile of neuroprotection to that of the previously reported analogues. Compounds **3c**, **3g**, **3h**, **3o**, **3p**, **3r**, and **5b** exhibited comparable neuroprotective activity of SH-SY5Y cells against $[Ca^{2+}]_c$ overload. Protective activities of new DHPs ranged from 22.1% (**3q**) to 40.1% (**3j**), and the best neuroprotection result was obtained with compound **3s**, which was able to prevent the death of 51% of cells. In general, compounds bearing an ester functionality showed a higher neuroprotective profile compared to those bearing a thioester moiety or polycyclic derivatives **5a** and **5b**, the latter of which had a low neuroprotective activity.

Taking into account compounds of type **3** studied, **3s**, bearing a 2-thienyl substituent at C-4, showed the best neuroprotective capability against $[Ca^{2+}]_c$ overload and **3q** showed the poorest profile. Generally, compounds bearing an electron-donating group were better neuroprotectants than those bearing an electron-withdrawing group.

VGCCs blockers have been previously studied as neuroprotectant agents, and as a common feature, it has been widely reported that their potency as $[Ca^{2+}]_c$ elevation blockers and the neuroprotective effect against Ca^{2+} overload are usually not correlated.[31] This characteristic is also relevant in our family of DHPs; i.e., compound **5b** showed the best Ca^{2+} signal blockade (79% blockade), but it showed a moderate activity as neuroprotectant in the $[Ca^{2+}]_c$ overload model. However, **3s** blocked 36% of the Ca^{2+} signal and protected 40% of cells. Similar results were obtained for compounds **3n** and **3j**, with 39% and 40% protection, respectively, which decreased only 43% and 48% the calcium increase elicited by 70 mM K^+ (Table 2). These results led us to focus our attention on the possibility of an additional mechanism of action for our compounds, possibly related to their antioxidant action, as previously described.[14] The correlation between Ca^{2+} influx through L-type VGCCs and increased mitochondrial oxidative stress has been recently reported.[32] Furthermore, L-type antagonists reverted the oxidative stress measured in the cells.[33] Therefore, the neuroprotective effect of our compounds against Ca^{2+} overload might be composed of VGCC blocker potency and antioxidant effect. The protective capabilities of these DHPs in an oxidative stress model are summarized in Table 5.

Neuroprotection: Oxidative Stress Model. Oxidative stress has been widely regarded as a key mechanism of neuronal death in several NDDs. As a common feature, high concentrations of reactive oxygen species (ROS) are produced by abnormal pathological mitochondria.[34] ROS oxidize lipids, causing membrane impairment and inducing cell death.[35] Oxidation would also affect ribosomal functioning and reduce protein synthesis.[36] Free radicals may also oxidize DNA and RNA, as shown by the detection of high levels of oxidized products in vulnerable neurons.

Rotenone and oligomycin A block complexes I and V, respectively, of the mitochondrial electron transport chain, thus disrupting ATP synthesis.[34] The mixture of rotenone plus oligomycin A (rot/olig) constitutes a good model of oxidative stress having its origin in mitochondria. Exposure to this combination induces neurotoxicity, and it has been widely used to evaluate potential protective drugs for neurodegenerative diseases.[37]

First, we were interested in assessing the potential antioxidant effect of compounds **3a**−**u** and **5a**,**b** with a co-incubation protocol. C5-unsubstituted DHPs were co-incubated for 8 h at a concentration of 5 μM with the stressor, followed by a 16 h postincubation of drugs at the same concentration without the toxic stimuli. These experimental conditions were designed to study the potential neuroprotective effect of the tested compounds based on their antioxidant capabilities. Besides, as described in the Introduction, oxidative stress may be increased by $[Ca^{2+}]_c$ overload;[22] thus, in the co-incubation model of oxidative stress, neuroprotection afforded by 5-unsubstituted DHPs could be dependent on their VGCC antagonism properties. Results are summarized in Table 5, compared with data for melatonin (0.3 μM) and nifedipine (5 μM), which were used as positive control and reference compound, respectively. Tested compounds showed, in general, interesting neuroprotective effects, ranging from 32.5% of derivative **3a** to 61.9% for **3e**, bearing an

dx.doi.org/10.1021/jm500263v | J. Med. Chem. 2014, 57, 4313−4323

Table 5. Neuroprotective Effect of C5-Unsubstituted DHPs 3a−u and 5a,b (5 μM) on SH-SY5Y Cell Viability against Toxicity Induced by (a) 8 h Co-Incubation of rot/olig Mixture (30/10 μM) in the Presence of Drugs, Followed by 16 h Postincubation of Drugs, or (b) 8 h Incubation of rot/olig Mixture without Any Drug, Followed by 16 h Postincubation of Drugs[a]

	8 h rot/olig co-incubation + 16 h postincubation		8 h rot/olig + 16 h postincubation	
compd	% survival	% protection	% survival	% protection
basal	100		100	
RO	65.6 ± 1.3$^{###}$		70.6 ± 1.8$^{###}$	
melatonin	82.5 ± 2.7***	44.7	87.8 ± 3.9**	58.3
nifedipine	78.4 ± 2.9**	29.3	73.8 ± 2.4^{ns}	11.7
3a	78.4 ± 3.4**	32.5		
3b	77.4 ± 5.9**	32.8		
3c	80.5 ± 2.9**	42.9	80.6 ± 3.3^{ns}	34.8
3d	79.5 ± 6.0**	39.6		
3e	87.3 ± 3.1***	61.9	76.7 ± 4.1^{ns}	21.7
3f	82.7 ± 3.2***	46.2		
3g	69.9 ± 3.9^{ns}	11.9		
3h	81.3 ± 7.0**	46.2	83.5 ± 2.2*	42.0
3i	82.3 ± 3.9***	45.7	81.8 ± 3.1^{ns}	38.6
3j	81.9 ± 3.4**	47.8	76.6 ± 3.9^{ns}	20.5
3k	85.7 ± 4.3***	57.9	74.2 ± 5.1^{ns}	12.3
3l	83.3 ± 4.2***	49.4	83.4 ± 3.1*	43.3
3m	79.9 ± 2.9**	36.2		
3n	83.5 ± 5.3**	53.3	88.0 ± 2.6**	60.1
3o	79.7 ± 3.2*	41.5	84.3 ± 3.1*	44.1
3p	64.6 ± 1.5^{ns}			
3q	69.9 ± 2.2^{ns}	11.7		
3r	60.0 ± 3.1^{ns}			
3s	81.9 ± 4.0***	45.3	77.5 ± 4.7^{ns}	25.6
3t	78.0 ± 3.6*	36.6	79.9 ± 3.8^{ns}	33.2
3u	83.7 ± 1.7***	52.4	86.2 ± 1.2**	52.2
5a	80.3 ± 3.9**	39.8		
5b	74.6 ± 4.3^{ns}	26.9		

[a]Data are the mean ± SEM of five to seven different cultures in triplicate. % protection was calculated considering MTT reduction by nontreated cells (basal) as 100% survival. % of toxicity was normalized for rot/olig seen for each treatment and subtracted to 100. (***) $p < 0.001$. (**) $p < 0.01$. (*) $p < 0.05$. ns = not significant with respect to rot/olig treated cells. (###) $p < 0.001$ compared to basal conditions. All compounds were assayed at 5 μM.

acetyl group instead of an ester or thioester substitution. In general, in a comparison of DHPs possessing the same substituents at positions 2, 3, and 6, ethyl ester and ketone derivatives showed similar protection profiles indicating that both groups have similar participation on their antioxidant effect. For the ethyl ester family, derivatives bearing electron-withdrawing groups were less potent neuroprotectants than those with electron-donating groups. Thus, compounds **3p** and **3r−q**, having respectively 4-NO_2 or 2-NO_2 groups, were the less active neuroprotectants in this model. On the other hand, methyl- and methoxyphenyl derivatives showed a protective effect over 40% in most cases, compound **3n** being the best with a 53.3% protection. Compounds bearing a *p*-chlorophenyl moiety at the C-6 position showed similar protection values as those compounds lacking this substituent, i.e., compounds **3h** (*p*-MeO-phenyl at C-4 and Ph at C-6) and **3j** (*m*-MeO-phenyl at C-4 and *p*-Cl-phenyl at C-6) with protection values of 46.2% and 47.8%, respectively. Regarding the C2-substituent, an increase of its steric volume was associated with an improvement of their neuroprotective profile, with protection values of 32.5% (Me, **3a**), 32.8% (Et, **3b**), and 42.9% (Pr, **3c**). A similar correlation was also observed for their antioxidant effect.

Regarding thioester derivatives, all tested compounds showed statistically significant neuroprotection with values ranging from 39.6% (**3d**) to 57.9% (**3k**). Compounds **3u** and **3k** afforded neuroprotective effects over 50%. Finally, polycyclic derivatives **5b** and **5a** were also able to protect SH-SY5Y cells in a statistically significant manner.

These encouraging results prompted us to study the compounds with the best overall neuroprotective profile on a second model of oxidative stress. A neuroprotective compound with potential therapeutic interest will be used clinically after neurons already have become vulnerable; for instance, diseases are diagnosed after neuronal damage has already been established.[38] Because we wanted to simulate experimental conditions closer to the clinical situation, in search for compounds able to protect cells already exposed to oxidative stress, we employed a protocol that consisted of an 8 h incubation period with the stressor, followed by a 16 h incubation period with the drug alone. We selected 11 DHPs to be tested in this postincubation oxidative stress model, and data are collected in Table 5. Melatonin (0.3 μM) and nifedipine (5 μM) were also tested as positive and reference compounds, respectively. Among all tested compounds, derivatives **3h**, **3l**, **3n**, **3o**, and **3u** demonstrated a neuroprotective effect after a 16 h postincubation in a statistically significant manner. Protection values were, in all cases, over 40%, ranging from 43.3% of derivative **3l** to the 60.1% protection afforded by compound **3n**. It is interesting to emphasize that nifedipine, which showed significant neuroprotection in the co-incubation stress model,

dx.doi.org/10.1021/jm500263v | J. Med. Chem. 2014, 57, 4313−4323

lost its ability to protect in the postincubation model. This result may indicate that neuroprotection is not fully dependent on the Ca^{2+} signal blockade properties. Finally, compound **3u**, being the second best antioxidant found in this model, also showed a good neuroprotective profile in the OGD model used previously.[14]

Neuroprotection: Oxygen–Glucose Deprivation of Hippocampal Slices. Acute Model of Ischemia/Reperfusion. Oxygen and glucose deprivation (OGD) is an acute model of the lesion produced by $[Ca^{2+}]_c$ overload during the OGD period followed by free radical generation during the reoxygenation phase.[39] In neurons, the OGD period depolarizes the membrane after mitochondrial failure. Depolarization induces substantial $[Ca^{2+}]_c$ elevation and a massive glutamate liberation, leading to increased cytotoxicity. Among all the experimental models of neurotoxicity elicited by Ca^{2+} overload, glutamate-induced Ca^{2+} overload seems to be the most relevant from a pathogenic point of view and has been related to several neurodegenerative diseases and stroke.[40] Additionally, recent observations have confirmed the influence of mitochondria-mediated cell Ca^{2+} regulation on glutamate-induced excitotoxicity.[41] On the other hand, the functional impairment of mitochondria, promoted by the lack of oxygen, is increased when reoxygenation triggers a massive production of reactive oxygen species raised by the OGD-induced overwork of the NADPH oxidase (NOX) enzyme.[42]

To further characterize the neuroprotective profile of compounds **3u** and **3n**, we used this model, where toxicity depends on $[Ca^{2+}]_c$ overload and oxidative stress. Rat hippocampal slices were subjected to 15 min OGD followed by 120 min reoxygenation (see protocol in Figure 3A), and cell viability was assessed by MTT reduction. Under these experimental conditions, slices were treated with **3n** or **3u** at increasing concentrations (1, 3, and 10 μM) and with nifedipine (10 μM) as a control. Considering cell viability in basal slices as 100%, OGD reduced cell viability by 40%.

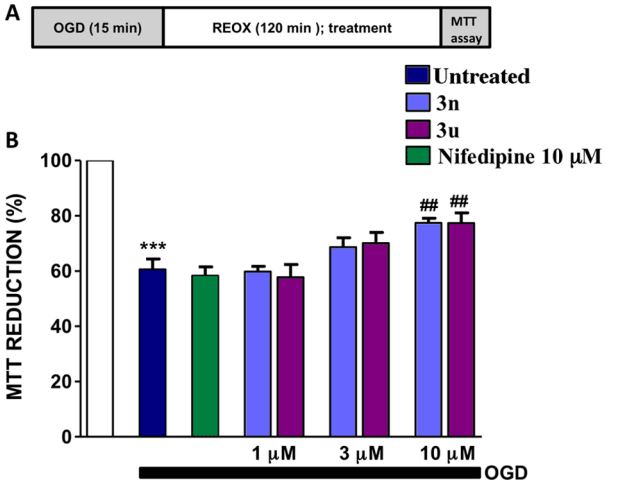

Figure 3. Post-OGD treatment with **3n** and **3u** protects hippocampal slices against oxygen and glucose deprivation followed by reoxygenation. (A) Protocol used to elicit toxicity. Hippocampal slices were exposed for 15 min to OGD followed by 2 h in control solution (Reox). **3n**, **3u** and nifedipine, when used, were present during the 2 h reox period. (B) Cell viability was measured by the MTT reduction activity. Values are expressed as the mean ± SEM of five independent experiments: (***) $p < 0.001$, compared to the basal; (##) $p < 0.01$ with respect to OGD-treated slices.

Compounds **3n** and **3u** afforded maximum protection at 10 μM (45%, Figure 3B). Nifedipine (10 μM) treatment produced no significant protection, corroborating the results obtained in SH-SY5Y cells subjected to rot/oligo stress postincubation.

CONCLUSION

In recent years, the different functions of $Ca_V1.2$ and $Ca_V1.3$ L-type VGCCs have attracted a great deal of attention because of their implication on different pathological conditions. In this line, we have prepared a new class of C5-unsubstituted-C6-aryl-1,4-dihydropyridines by a CAN-catalyzed multicomponent reaction from chalcones, β-dicarbonyl compounds, and ammonium acetate. These compounds were able to block Ca^{2+} entry after a depolarizing stimulus and showed an improved $Ca_V1.3/Ca_V1.2$ selectivity, when compared to classical dihydropyridines. Docking studies have led to some interesting conclusions on the interactions with the $Ca_V1.2$ channel that will be of interest for the future development of a new generation of C5-unsubstituted 1,4-dihydropyridines. Our DHPs protected neuroblastoma cells against $[Ca^{2+}]_c$ overload and oxidative stress-induced toxicity. Their selectivity ratio makes them highly interesting for the treatment of neurological disorders where Ca^{2+} dyshomeostasis and high levels of oxidative stress have been demonstrated, since their low potency toward the cardiovascular channel subtype makes them potentially safer than classical 1,4-dihydropyridines as far as cardiovascular side effects are concerned. Some compounds afforded good protection in a postincubation model, which better simulates the clinical condition, offering a therapeutic window of opportunity of great interest for patient recovery after a brain ischemic episode. Good activities were also found in acute ischemia/reperfusion (oxygen and glucose deprivation) models. Taken together, these compounds deserve further investigation on neurological disease animal models to confirm their good in vitro neuroprotective profile described here.

EXPERIMENTAL SECTION

Chemistry. The purity of new compounds was determined by CHNS elemental analysis, and all values were verified to be within 0.4% of theoretical data.

General Procedure for the Synthesis of 1,4-Dihydropyridine Derivatives (3) and 4,6,7,8-Tetrahydroquinolin-5(1*H*)-ones (5). To a stirred solution of 1,3-diphenyl-2-propen-1-one derivatives (1 equiv, 2 mmol), 1,3-dicarbonyl compounds (1.1 equiv, 2.2 mmol), and ammonium acetate (3 equiv, 6 mmol) in ethanol (3 mL) was added ceric ammonium nitrate (CAN, 10% mol), and the resulting mixture was refluxed for 4 h. After this time, ammonium acetate (1.5 equiv, 3 mmol) was again added and stirring was continued at the same conditions for additional 4 h. After completion of the reaction (checked by TLC), the mixture was allowed to cool to room temperature, diluted with CH_2Cl_2 (20 mL), and washed with water to remove CAN and the excess of ammonium acetate. The organic layer was then washed with brine and dried over anhydrous Na_2SO_4, and the solvent was evaporated under reduced pressure. The crude residue was crystallized from EtOH or purified by silica gel column chromatography using a petroleum ether–ethyl acetate mixture (12:1 v/v) as eluent to give pure compounds (**3a–u** or **5a,b**). Characterization data for representative compounds follow. For full characterization data, see the Supporting Information.

Ethyl 4,6-Diphenyl-2-propyl-1,4-dihydropyridine-3-carboxylate (3c). Yellow paste; ^1H NMR ($CDCl_3$, 250 MHz) δ 1.08 (t, J = 7.3 Hz, 3H, $CH_2CH_2CH_3$), 1.17 (t, J = 7.1 Hz, 3H, OCH_2CH_3), 1.69–1.84 (m, 2H, $CH_2CH_2CH_3$), 2.69–2.90 (m, 2H, $CH_2CH_2CH_3$), 4.06 (q, J = 7.1 Hz, 2H, OCH_2CH_3), 4.73 (d, J = 5.6 Hz, 1H, C-4*H*), 5.20–5.23 (dd, J = 1.9, 5.6 Hz, 1H, C-5*H*), 5.68 (bs, 1H, N*H*), 7.15–7.43 (m, 10H, Ar*H*); ^{13}C NMR ($CDCl_3$, 63 MHz) δ 14.60

dx.doi.org/10.1021/jm500263v | J. Med. Chem. 2014, 57, 4313–4323

($CH_2CH_2CH_3$), 14.64 (OCH_2CH_3), 22.7 ($CH_2CH_2CH_3$), 36.1 ($CH_2CH_2CH_3$), 41.4 (C-4), 59.7 (OCH_2CH_3), 99.0 (C-3), 105.4(C-5), 125.5 (2xCHAr), 126.4 (CHAr), 128.1 (2 × CHAr), 128.6 (2 × CHAr), 128.9 (CHAr), 129.2 (2 × CHAr), 134.6, 136.4 (C-6CAr, C-6), 149.4, 151.6 (C-4CAr, C-2), 168.5 (COOR); IR (NaCl) ν 3363, 2963, 2933, 2872, 1724, 1602, 1576, 1494, 1448, 1411, 1273, 1216, 1098, 698 cm^{-1}; elemental analysis calcd (%) for $C_{23}H_{25}NO_2$, C 79.51, H 7.25, N 4.03; found, C 79.21, H 6.93, N 3.94.

Ethyl 4,6-Bis(4-chlorophenyl)-2-methyl-1,4-dihydropyridine-3-carboxylate (3g). Yellow solid, mp >250 °C; ^1H NMR ($CDCl_3$, 250 MHz) δ 1.17 (t, J = 7.1 Hz, 3H, OCH_2CH_3), 2.44 (s, 3H, C-2CH_3), 4.05 (q, J = 7.1 Hz, 2H, OCH_2CH_3), 4.69 (d, J = 5.5 Hz, 1H, C-4H), 5.15 (dd, J = 1.88, 5.5 Hz, 1H, C-5H), 5.57 (bs, 1H, NH), 7.26 (s, 4H, ArH), 7.35 (s, 4H, ArH); ^{13}C NMR ($CDCl_3$, 63 MHz) δ 14.7 (OCH_2CH_3), 21.1 (C-2CH_3), 40.8 (C-4), 59.8 (OCH_2CH_3), 99.4 (C-3), 105.5 (C-5), 126.8 (2 × CHAr), 128.8 (2 × CHAr), 129.4 (2 × CHAr), 129.5 (2 × CHAr), 132.1, 134.0, 134.6, 134.8 (C-6CAr, C-6, 2 × ArCCl), 147.3, 147.5 (C-4CAr, C-2), 168.5 (COOR); IR (NaCl) ν 3348, 2982, 1724, 1597, 1491, 1270, 1231, 1091, 1015, 757 cm^{-1}; elemental analysis calcd (%) for $C_{21}H_{19}Cl_2NO_2$, C 64.96, H 4.93, N 3.61; found, C 64.78, H 4.84, N 3.43.

Ethyl 6-(4-Chlorophenyl)-4-(3-methoxyphenyl)-2-methyl-1,4-dihydropyridine-3-carboxylate (3j). Yellow syrup; ^1H NMR ($CDCl_3$, 250 MHz) δ 1.17 (t, J = 7.12 Hz, 3H, OCH_2CH_3), 2.44 (s, 3H, C-2CH_3), 3.81 (s, 3H, OCH_3), 4.08 (q, J = 7.12 Hz, 2H, OCH_2CH_3), 4.69 (d, J = 5.5 Hz, 1H, C-4H), 5.19 (dd, J = 1.2, 5.5 Hz, 1H, C-5H), 5.54 (bs, 1H, NH), 6.72−6.77 (dd, J = 2.5, 8.1 Hz, 1H, C-4ArH), 6.89−6.96 (m, 2H, C-4ArH), 7.23 (t, J = 7.8 Hz, 1H, C-4ArH), 7.35 (s, 4H, C-6ArH); ^{13}C NMR ($CDCl_3$, 63 MHz) δ 14.7 (OCH_2CH_3), 21.1 (C-2CH_3), 41.3 (C-4), 55.5 (OCH_3), 59.7 (OCH_2CH_3), 99.6 (C-3), 105.9 (C-5), 111.4 (CHAr), 114.2 (CHAr), 120.6 (CHAr), 126.8 (2 × CHAr), 129.3(2 × CHAr), 129.6 (CHAr), 133.8, 134.7, 134.8 (C-6CAr, C-6, ArCCl), 147.1, 150.7 (C-4CAr, C-2), 160.0 (ArC-OCH_3), 168.6 (COOR); IR (NaCl) ν 3356, 2980, 1724, 1676, 1596, 1486, 1286, 1266, 1224, 1093, 754 cm^{-1}; elemental analysis calcd (%) for $C_{22}H_{22}ClNO_3$, C 68.83, H 5.78, N 3.65; found, C 68.59, H 5.67, N 3.72.

Allyl 6-(4-Chlorophenyl)-2-methyl-4-phenyl-1,4-dihydropyridine-3-carboxylate (3o). Orange syrup; ^1H NMR ($CDCl_3$, 250 MHz) δ 2.45 (s, 3H, C-2CH_3), 4.52 (dd, J = 0.85, 5.3 Hz 2H, $OCH_2CH{=}CH_2$), 4.74 (d, J = 5.58 Hz, 1H, C-4H), 5.10−5.23 (m, 3H, C-5H, $OCH_2CH{=}CH_2$), 5.60 (bs, 1H, NH) 5.76−5.93 (m, 1H, $OCH_2CH{=}CH_2$), 7.17−7.24 (m, 1H, ArH), 7.28−7.38 (m, 8H, ArH); ^{13}C NMR ($CDCl_3$, 63 MHz) δ 18.8 (C-2CH_3), 38.8 (C-4), 62.1 ($OCH_2CH{=}CH_2$), 96.8 (C-3), 103.7 (C-5), 115.0 ($OCH_2CH{=}CH_2$), 124.2 (CHAr), 124.4 (2 × CHAr), 125.6 (2 × CHAr), 126.3 (2 × CHAr), 130.9 ($OCH_2CH{=}CH_2$), 131.2, 132.2, 132.3 (C-6CAr, C-6, ArCCl), 145.2, 146.4 (C-4CAr, C-2), 165.8 (COOR); IR (NaCl) ν 3342, 2926, 1678, 1606, 1484, 1221, 1095 cm^{-1}; elemental analysis calcd (%) for $C_{22}H_{20}ClNO_2$, C 72.22, H 5.51, N 3.83; found, C 71.97, H 5.43, N 4.00.

Ethyl 2-Methyl-4-(2-nitrophenyl)-6-(4-tolyl)-1,4-dihydropyridine-3-carboxylate (3q). Yellow syrup; ^1H NMR ($CDCl_3$, 250 MHz) δ 0.98 (t, J = 7.1 Hz, 3H, OCH_2CH_3), 2.38 (s, 3H, CH_3), 2.49 (s, 3H, CH_3), 3.92 (q, J = 7.1 Hz, 2H, OCH_2CH_3), 5.21 (d, J = 5.05 Hz, 1H, C-4H), 5.38 (dd, J = 1.8, 5.05 Hz, 1H, C-5H), 5.67 (bs, 1H, NH), 7.19 (d, J = 7.95 Hz, 2H, C-6ArH), 7.25−7.33 (m, 3H, ArH), 7.55 (dt, J = 1.0, 7.42 Hz, 1H, C-4ArH), 7.66 (dd, J = 1.22, 7.87 Hz, 1H, C-4ArH), 7.74 (dd, J = 1.0, 8.08 Hz, 1H, C-4ArH); ^{13}C NMR ($CDCl_3$, 63 MHz) δ 14.3 (OCH_2CH_3), 20.8 (CH_3), 21.6 (CH_3), 31.1 (C-4), 59.7 (OCH_2CH_3), 98.5 (C-3), 103.6 (C-5), 123.5 (CHAr), 125.3 (2 × CHAr), 126.7 (CHAr), 129.9 (2 × CHAr), 131.9 (CHAr), 133.0, 133.5, 135.1 (C-6CAr, CHAr, C-6), 144.1, 148.2, 148.9 (C-4CAr, C-2, $ArCNO_2$), 168.0 (COOR); IR (NaCl) ν 3332, 2976, 1674, 1608, 1524, 1486, 1355, 1221, 1084, 750 cm^{-1}; elemental analysis calcd (%) for $C_{22}H_{22}N_2O_4$, C 69.83, H 5.86, N 7.40; found, C 69.86, H 5.69, N 7.64.

Ethyl 6-(4-Chlorophenyl)-2-methyl-4-(2-nitrophenyl)-1,4-dihydropyridine-3-carboxylate (3r). Yellow syrup; ^1H NMR ($CDCl_3$, 250 MHz) δ 0.97 (t, J = 7.1 Hz, 3H, OCH_2CH_3), 2.49 (s, 3H, C-2CH_3), 3.91 (q, J = 7.1 Hz, 2H, OCH_2CH_3), 5.21 (d, J = 5.1 Hz, 1H, C-4H), 5.40 (dd, J = 1.7, 5.1 Hz, 1H, C-5H), 5.57 (bs, 1H, NH), 7.27−7.34 (m, 1H, ArH), 7.36 (s, 4H, ArH), 7.53−7.66 (m, 2H, ArH), 7.76 (dd, J = 1, 8.2 Hz, 1H, C-4ArH); ^{13}C NMR ($CDCl_3$, 63 MHz) δ 14.3 (OCH_2CH_3), 20.8 (C-2CH_3), 37.2 (C-4), 59.8 (OCH_2CH_3), 98.7 (C-3), 104.7 (C-5), 123.6 (CHAr), 126.8 (2 × CHAr), 127.1 (CHAr), 129.4 (2 × CHAr), 131.8 (CHAr), 133.6 (CHAr), 134.3, 134.4, 135.0 (C-6CAr, C-6, ArCCl), 143.7, 148.2, 148.7 (C-4CAr, C-2, $ArCNO_2$), 167.8 (COOR); IR (NaCl) ν 3188, 1721, 1651, 1610, 1528, 1482, 1439, 1269, 1094, 826, 747 cm^{-1}; elemental analysis calcd (%) for $C_{21}H_{19}ClN_2O_4$, C 69.22, H 5.53, N 7.69; found, C 69.11, H 5.37, N 7.66.

Ethyl 6-(Furan-2-yl)-2-methyl-4-(4-tolyl)-1,4-dihydropyridine-3-carboxylate (3t). Yellow syrup; ^1H NMR ($CDCl_3$, 250 MHz) δ 1.18 (t, J = 7.1 Hz, 3H, OCH_2CH_3), 2.32 (s, 3H, CH_3), 2.44 (s, 3H, CH_3), 4.05 (q, J = 7.1 Hz, 2H, OCH_2CH_3), 4.64 (d, J = 5.65 Hz, 1H, C-4H), 5.37 (dd, J = 1.58, 5.65 Hz, 1H, C-5H), 5.90 (bs, 1H, NH), 6.40−6.44 (m, 2H, furylH), 7.10 (d, J = 8.02 Hz, 2H, C-4ArH), 7.23 (d, J = 8.02 Hz, 2H, C-4ArH), 7.39−7.40 (m, 1H, furylH); ^{13}C NMR ($CDCl_3$, 63 MHz) δ 14.7 (OCH_2CH_3), 21.1 (CH_3), 21.5 (CH_3), 40.1 (C-4), 59.7 (OCH_2CH_3), 99.7, 103.4 (C-3, C-5), 105.1 (CH-furyl), 112.0 (CH-furyl), 126.3 (C-6), 128.1 (2 × CHAr), 129.4 (2 × CHAr), 136.0 ($ArCCH_3$), 141.9 (CH-furyl), 146.0, 146.6, 149.1 (C-4CAr, C-2, C-furyl), 168.7 (COOR); IR (NaCl) ν 3348, 2980, 1724, 1662, 1604, 1268, 1096, 751 cm^{-1}; elemental analysis calcd (%) for $C_{20}H_{21}NO_3$, C 74.28, H 6.55, N 4.33; found, C 73.99, H 6.37, N 4.22.

Docking Calculations. The crystal structure of the $Ca_V1.2$ L-subtype VGCC has not been described, and therefore, for molecular modeling studies we used the $Ca_V1.2$ L-subtype VGCC model developed by D. Tikhonov and B. S. Zhorov and kindly shared with us by Prof. Zhorov.[24] Docking was performed with the program Molegro Virtual Docker[43] using the molecular docking algorithm Moldock score. Prior to docking, the structures of nifedipine and (*S*)-**3n** were built and their energies were minimized using Gaussian software (Frisch, M. J.; et al. *Gaussian 03*, revision B.04; Gaussian, Inc.: Pittsbusrg, PA, 2003). Calculations were run on an iMac with a 3.4 GHz i7 processor and 16 GB DDR3. Ligand binding cavities were identified using the Molegro expanded van der Waals molecular surface prediction algorithm with a grid resolution of 0.5 Å. A total of 100 docking runs with a population size of 100 were calculated over a 16 Å radius surrounding the predicted DHP binding site cavity with a grid resolution of 0.3, a maximum of 15 000 iterations per position, a scaling factor of 0.50, and crossover rate of 0.90 using the Moldock score algorithm. Moldock optimizer function was used to more precisely optimize H-bond geometries by calculating the position of the hydrogen atoms for any hydrogen donors (both in the ligand and in the proteins). Similar positions were clustered using a root mean squared deviation (rmsd) of 1.5 Å. Prepositioned ligands were randomized in the predicted cavity prior to each docking run, and docking was constrained to the predicted DHPs binding site cavity. In order to verify that positions resulting from in silico docking represent correctly bound conformations, each position was visually inspected and compared. Positions were also inspected and compared with the rerank score algorithm, protein interaction, hydrogen bonding, and affinity interaction energies and ordered by the energy of interaction protein−ligand. Complexes were optimized using Moloc software[44] (www.moloc.ch) with standard force field and optimization parameters. During energy minimization the position of amino acid side chains were fixed while allowing all ligand atoms to move.

Pharmacology. SH-SY5Y Neuroblastoma Cells Culture. SH-SY5Y cells were cultured following supplier instructions in a 1:1 mixture of F12 (Ham 12) and Eagle's MEM supplemented with 15 nonessential amino acids, 10% heat-inactivated fetal bovine serum (FBS), 1 mM sodium pyruvate, 100 μg/mL streptomycin, and 100 units/mL penicillin. Cells were kept at 37 °C in a humidified atmosphere of 95% air and 5% CO_2. For experimental procedures, cells were cultured in 48-well plates at a density of 1×10^5 cells/well. Treatments were performed in 1% FBS medium unless other concentration is stated. Cells were used up to 13 passages.

Ca^{2+} Signal Measurements. Neuroblastoma cells were cultured in bottom-transparent black 96-well plates at a density of 5×10^4 cells/well. After 2 days in culture, cells were loaded with 10 μM Fluo-4/AM for 1 h at 37 °C in culture medium without FBS. After loading period, cells were washed twice with Krebs-HEPES solution and kept at room temperature for 15 min before starting the experiment. Compounds at the desired concentration were incubated for 15 min before injecting the stimulus (70 mM KCl). Fluorescence intensity was measured for 12 s at 485 and 520 nm wavelengths of excitation and emission, respectively, in a microplate reader (FLUOstar Optima, BMG, Offenburg, Germany). Once the experiment was finish, 50 μL of Triton (5%) was added to measure maximum fluorescence (F_{max}), followed by 50 μL of $MnCl_2$ to obtain the minimum fluorescence (F_{min}). Potassium evoked responses were expressed as % of fluorescence at each time point (F) minus minimum fluorescence values divided by $F_{max} - F_{min}$. The maximum value of F_{520} obtained for each well was considered as the peak F_{520} value.

Neuroprotection against Ca^{2+} Overload Induced by High K^+. Stock solutions of the compounds under assay were prepared in DMSO at 10^{-2} M concentration and kept at −20 °C. Compounds were diluted with neuroblastoma cells culture medium to the desired concentration (5 μM), and cells were co-incubated for 24 h with the toxic stimulus. The control group was treated with the same amount of DMSO alone.

Neuroprotection against Oxidative Stress Induced by Rotenone−Oligomycin A Cocktail. *(a) Co-Incubation Protocol.* Compounds were diluted from stock solutions with neuroblastoma cells culture media (1% FBS) containing the rotenone−oligomycin A mixture (30 μM/10 μM, respectively) to the desired concentration (5 μM). Then cells were co-incubated for 24 h with each treatment and toxic stimulus rot/olig. Control cells were treated with the same concentration of DMSO without any drug. Melatonin (0.3 μM) and nifedipine (5 μM) were used as positive and reference controls, respectively.

(b) Postincubation Protocol. Cells were cultured for 24 h. Culture medium was replaced by media containing toxic stimulus cocktail (rot/olig 30/10 μM), and cells were incubated for 8 h at 37 °C. Thereafter, compounds were diluted from stock solutions with neuroblastoma cell culture medium (1% FBS) to the desired concentration (5 μM). Then cells were incubated for 16 h with each treatment and without toxic stimulus. Control cells were treated with the same concentration of DMSO without any drug. Melatonin and nifedipine were used as positive and reference controls, respectively.

Animal Usage and Hippocampal Slice Preparation. The experiments were performed after protocol approval by the institutional Ethic Committee of the Universidad Autónoma de Madrid, Spain, according to the European Guideline for the Use and Care of Animals for Research. All efforts were made to minimize animal suffering and to reduce the number of animals used in the experiments.

Experiments were completed in hippocampal slices from adult male Sprague−Dawley rats (275−325 g). The protocol for hippocampal slice preparation was similar to that used by Egea et al.[39] with slight modifications. After quick decapitation of rats (pentobarbital anesthesia, 60 mg/kg ip), forebrains were rapidly removed and kept in ice-cold Krebs bicarbonate dissection buffer (pH 7.4) (in mM): KCl, 2; NaCl, 120; $CaCl_2$, 0.5; $NaHCO_3$, 26; $MgSO_4$, 10; KH_2PO_4, 1.18; glucose, 11; sucrose, 200. Then dissected hippocampi were quickly glued down leaning vertically against agar blocks in small chamber, submerged in cold, oxygenated dissection buffer, and sectioned in transverse slices of 200 μM thick using a vibratome (Leica, Hidelberg, Germany).

Neuroprotection against Oxidative Stress Induced by Oxygen and Glucose Deprivation (OGD) in Hippocampal Slices. We have used a previously described protocol.[39] Solutions were prebubbled with either 95% O_2/5% CO_2 or 95% N_2/5% CO_2 gas mixtures for 45 min before slice immersion to ensure O_2 or N_2 saturation. After a stabilization period of 30 min, hippocampal slices of the control group were incubated for 15 min in Krebs solution equilibrated with 95% O_2/5% CO_2 at 37 °C. OGD was achieved by incubating the hippocampal slices in a glucose-free Krebs solution equilibrated with 95% N_2/5% CO_2 at 37 °C over 15 min. Glucose was replaced by 2-deoxyglucose. After a 15 min OGD period, slices were reincubated in oxygenated normal Krebs solution for 120 min (reoxygenation period) at 37 °C.

Viability Quantification by MTT Reduction in SH-SY5Y Neuroblastoma Cells and Hippocampal Slices. Cell viability was measured by MTT reduction, which measures the mitochondrial activity of living cells, by quantitative colorimetric assay.[45] Briefly, MTT was added to each well at a final concentration of 5 mg/mL and incubated at 37 °C in the dark for 2 h. Then the culture medium was eliminated and the precipitate was dissolved by adding 300 μL/well (48-well plate) of DMSO. An amount of 100 μL of the resulting colored solution from each well was transferred to a transparent 96-well plate, and optical density was measured in an ELISA reader at 540 nm. Control cells treated with DMSO were taken as 100% viability. Hippocampal cell viability was determined using the same colorimetric probe.

Hippocampal slices were immediately transferred to a 96-well plate after reoxygenation and incubated with MTT at a final concentration of 0.5 mg/mL in Krebs bicarbonate solution for 30 min at 37 °C. Finally, the precipitate was dissolved in 200 μL of DMSO and optical density was measured. Absorbance of control slices was taken as 100% viability.

Vascular Reactivity. Third order branches of mesenteric artery from 6-month-old Wistar Kyoto rats (2 mm length) were mounted in a small-vessel dual chamber myograph to monitor isometric tension. Two steel wires (40 μm diameter) were introduced through the lumen of the segments and mounted as previously described.[46] After a 30 min equilibration period in oxygenated Krebs−Henseleit solution (KHS) at 37 °C (pH 7.4), segments were stretched to their optimal lumen diameter for active tension development.[46] Then segments were washed with KHS and equilibrated for 30 min. Contractility of segments was then tested by an initial exposure to a high-K^+ solution (120 mM KCl−KHS). The presence of endothelium was determined by the ability of 10 μM acetylcholine to induce relaxation in arteries precontracted with phenylephrine at a concentration that produces approximately 50% of the contraction induced by KCl−KHS. In different segments, concentration−response curves (0.01 nM to 0.1 μM) to nifedipine, **3n**, **3u**, and **5b** were performed in arteries precontracted with a 70 mM KCl−KHS solution.

Statistical Analysis. All values are expressed as the mean ± SEM, and "n" represents the number of different cultures or animals used. The IC_{50} or EC_{50} values were calculated by nonlinear regression analysis of each individual concentration−response curve using GraphPad Prism software (San Diego, CA, USA). Results were analyzed using comparisons between experimental and control groups performed by one-way ANOVA followed by Newman-Keuls post hoc test. Differences were considered to be statistically significant when $p \leq 0.05$.

■ ASSOCIATED CONTENT

Ⓢ Supporting Information

General experimental methods in chemistry, reaction conditions, compound characterization, NMR spectra, and pharmacology protocols used. This material is available free of charge via the Internet at http://pubs.acs.org.

■ AUTHOR INFORMATION

Corresponding Authors

*R.L.: fax, 34-91-4973543; phone, 34-91-4972766; e-mail, rafael.leon@uam.es.

*J.C.M.: fax, 34-91-3941822; phone, 34-91-3941840; e-mail, josecm@farm.ucm.es.

Author Contributions

#G.T. and E.S. contributed equally.

G.T. participated in the design and synthesis of new DHPs and drafting and critical revision of the manuscript. E.P.

participated in the design of pharmacological experiments, data acquisition and analysis of neuroprotection experiments, and critical revision of the manuscript. S.M.-R. and A.M.B. contributed to data acquisition and data analysis/interpretation and critical revision of the manuscript. J.E. and M.G.L. contributed to pharmacological data analysis/interpretation and critical revision of the manuscript. V.S. participated in the design and synthesis of new DHPs. M.T.R. contributed to the design and synthesis supervision of new DHPs, data analysis/interpretation, and critical revision of the manuscript. R.L. contributed to concept/design, acquisition of data and analysis of VGCCs blockade IC_{50} calculation and molecular modeling, drafting of the manuscript, critical revision of the manuscript, and approval of the article. J.C.M. contributed to concept/design, synthesis supervision, drafting of the manuscript, critical revision of the manuscript, and approval of the article.

Notes

The authors declare no competing financial interest.

■ ACKNOWLEDGMENTS

Prof. Boris Zhorov is gratefully acknowledged for providing the $Ca_V1.2$ PDB model used in molecular modeling. R.L. thanks Instituto de Salud Carlos III for a research contract under the Miguel Servet Program (Grant CP11/00165). G.T. thanks Universidad Complutense for a predoctoral fellowship. A.M.B. thanks MINECO for a research contract under the Ramón y Cajal program (Grant RyC-2010-06473). We also thank the continued support of Fundación Teófilo Hernando, Madrid, Spain. Financial support came from the following: Spanish Ministerio de Economía y Competitividad, MINECO (Grants CTQ-2012-33272 to J.C.M. and SAF-2012-32223 to M.G.L.); People Programme (Marie Curie Actions) of the European Union's Seventh Framework Programme (FP7/2007−2013) under REA Grant PCIG11-GA-2012-322156 to R.L.; IS Carlos III, Programa Miguel Servet (Grant CP11/00165) to R.L.; IS Carlos III (Grant PI13/01488 to A.M.B.), and the Spanish Ministry of Health (Instituto de Salud Carlos III) Grant RENEVAS-RETICS-RD06/0026 to M.G.L.

■ ABBREVIATIONS USED

CAN, ceric ammonium nitrate; $[Ca^{2+}]_c$, cytosolic calcium concentration; $Ca_V1.3$, L-type voltage-gated calcium channel 1.3; $Ca_V1.2$, L-type voltage-gated calcium channel 1.2; DHP, 1,4-dihydropyridine; NDD, neurodegenerative disease; OGD, oxygen and glucose deprivation; ROS, reactive oxygen species; rot/olig, mixture of 30 μM rotenone and 10 μM oligomycin A; SAR, structure−activity relationship; SNc, substantia nigra pars compacta; VGCC, voltage-gated calcium channel.

■ REFERENCES

(1) Jaffer, H.; Morris, V. B.; Stewart, D.; Labhasetwar, V. Advances in stroke therapy. *Drug Delivery Transl. Res.* **2011**, *1*, 409−419.

(2) (a) Jellinger, K. A. General aspects of neurodegeneration. *J. Neural Transm., Suppl.* **2003**, 101−144. (b) Szydlowska, K.; Tymianski, M. Calcium, ischemia and excitotoxicity. *Cell Calcium* **2010**, *47*, 122−129.

(3) Auriel, E.; Bornstein, N. M. Neuroprotection in acute ischemic stroke—current status. *J. Cell. Mol. Med.* **2010**, *14*, 2200−2202.

(4) Gribkoff, V. K.; Winquist, R. J. Voltage-gated cation channel modulators for the treatment of stroke. *Expert Opin. Invest. Drugs* **2005**, *14*, 579−592.

(5) (a) Lipscombe, D.; Helton, T. D.; Xu, W. L-type calcium channels: the lowdown. *J. Neurophysiol.* **2004**, *92*, 2633−2641. (b) Triggle, D. J. L-type calcium channels. *Curr. Pharm. Des.* **2006**, *12*, 443−457.

(6) Catterall, W. A.; Perez-Reyes, E.; Snutch, T. P.; Striessnig, J. International Union of Pharmacology. XLVIII. Nomenclature and structure−function relationships of voltage-gated calcium channels. *Pharmacol. Rev.* **2005**, *57*, 411−425.

(7) Halling, D. B.; Aracena-Parks, P.; Hamilton, S. L. Regulation of voltage-gated Ca^{2+} channels by calmodulin. *Sci. STKE* **2005**, *2005*, re15.

(8) Striessnig, J.; Koschak, A. Exploring the function and pharmacotherapeutic potential of voltage-gated Ca^{2+} channels with gene knockout models. *Channels (Austin)* **2008**, *2*, 233−251.

(9) (a) Chan, C. S.; Guzmán, J. N.; Ilijic, E.; Mercer, J. N.; Rick, C.; Tkatch, T.; Meredith, G. E.; Surmeier, D. J. "Rejuvenation" protects neurons in mouse models of Parkinson's disease. *Nature* **2007**, *447*, 1081−1086. (b) Hurley, M. J.; Brandon, B.; Gentleman, S. M.; Dexter, D. T. Parkinson's disease is associated with altered expression of CaV1 channels and calcium-binding proteins. *Brain* **2013**, *136*, 2077−2097.

(10) Kang, S.; Cooper, G.; Dunne, S. F.; Dusel, B.; Luan, C. H.; Surmeier, D. J.; Silverman, R. B. CaV1.3-selective L-type calcium channel antagonists as potential new therapeutics for Parkinson's disease. *Nat. Commun.* **2012**, *3*, 1146.

(11) (a) Edraki, N.; Mehdipour, A. R.; Khoshneviszadeh, M.; Miri, R. Dihydropyridines: evaluation of their current and future pharmacological applications. *Drug Discovery Today* **2009**, *14*, 1058−1066. (b) Ioan, P.; Carosati, E.; Micucci, M.; Cruciani, G.; Broccatelli, F.; Zhorov, B. S.; Chiarini, A.; Budriesi, R. 1,4-Dihydropyridine scaffold in medicinal chemistry, the story so far and perspectives (part 1): action in ion channels and GPCRs. *Curr. Med. Chem.* **2011**, *18*, 4901−4922.

(12) Striessnig, J.; Koschak, A.; Sinnegger-Brauns, M. J.; Hetzenauer, A.; Nguyen, N. K.; Busquet, P.; Pelster, G.; Singewald, N. Role of voltage-gated L-type Ca^{2+} channel isoforms for brain function. *Biochem. Soc. Trans.* **2006**, *34*, 903−909.

(13) (a) Kang, S.; Cooper, G.; Dunne, S. F.; Luan, C. H.; Surmeier, D. J.; Silverman, R. B. Structure−activity relationship of N,N′-disubstituted pyrimidinetriones as Ca(V)1.3 calcium channel-selective antagonists for Parkinson's disease. *J. Med. Chem.* **2013**, *56*, 4786−4797. (b) Locatelli, A.; Cosconati, S.; Micucci, M.; Leoni, A.; Marinelli, L.; Bedini, A.; Ioan, P.; Spampinato, S. M.; Novellino, E.; Chiarini, A.; Budriesi, R. Ligand based approach to L-type calcium channel by imidazo[2,1-*b*]thiazole-1,4-dihydropyridines: from heart activity to brain affinity. *J. Med. Chem.* **2013**, *56*, 3866−3877. (c) Chang, C. C.; Cao, S.; Kang, S.; Kai, L.; Tian, X.; Pandey, P.; Dunne, S. F.; Luan, C. H.; Surmeier, D. J.; Silverman, R. B. Antagonism of 4-substituted 1,4-dihydropyridine-3,5-dicarboxylates toward voltage-dependent L-type Ca^{2+} channels Ca_V 1.3 and Ca_V 1.2. *Bioorg. Med. Chem.* **2010**, *18*, 3147−3158.

(14) Tenti, G.; Egea, J.; Villarroya, M.; León, R.; Fernández, J. C.; Padín, J. F.; Sridharan, V.; Ramos, M. T.; Menéndez, J. C. Identification of 4,6-diaryl-1,4-dihydropyridines as a new class of neuroprotective agents. *MedChemComm* **2013**, *4*, 590−594.

(15) Triggle, D. J. 1,4-Dihydropyridines as calcium channel ligands and privileged structures. *Cell. Mol. Neurobiol.* **2003**, *23*, 293−303.

(16) For a review, see the following: Sridharan, V.; Menéndez, J. C. Cerium(IV) ammonium nitrate as a catalyst in organic synthesis. *Chem. Rev.* **2010**, *110*, 3805−3849.

(17) Safari, J.; Banitaba, S. H.; Khalili, S. D. Cellulose sulfuric acid catalyzed multicomponent reaction for efficient synthesis of 1,4.dihydropyridines via unsymmetrical Hantzsch reaction in aqueous media. *J. Mol. Catal. A: Chem.* **2011**, *335*, 46−50.

(18) Rehberg, R.; Kroehnke, F. Michale-additionen von 1,3-diketonen an α,β-ungesattigte ketone. *Liebigs Ann. Chem.* **1968**, *717*, 91−95.

(19) Kuno, A.; Sakai, H.; Sugiyama, Y.; Takasugi, H. Studies on cerebral protective agents. IV. Synthesis of novel 4-arylpyridine and 4-arylpyridazine derivatives with anti-anoxic activity. *Chem. Pharm. Bull. (Tokyo)* **1993**, *41*, 156−162.

(20) Kumar, A.; Sharma, S.; Tripathi, V. D.; Maurya, R. A.; Srivastava, S. P.; Bhatia, G.; Tamrakar, A. K.; Srivastava, A. K. Design and

synthesis of 2,4-disubstituted polyhydroquinolines as prospective antihyperglycemic and lipid modulating agents. *Bioorg. Med. Chem.* **2010**, *18*, 4138−4148.
(21) Sinnegger-Brauns, M. J.; Huber, I. G.; Koschak, A.; Wild, C.; Obermair, G. J.; Einzinger, U.; Hoda, J. C.; Sartori, S. B.; Striessnig, J. Expression and 1,4-dihydropyridine-binding properties of brain L-type calcium channel isoforms. *Mol. Pharmacol.* **2009**, *75*, 407−414.
(22) Guzmán, J. N.; Sánchez-Padilla, J.; Wokosin, D.; Kondapalli, J.; Ilijic, E.; Schumacker, P. T.; Surmeier, D. J. Oxidant stress evoked by pacemaking in dopaminergic neurons is attenuated by DJ-1. *Nature* **2010**, *468*, 696−700.
(23) Sousa, S. R.; Vetter, I.; Ragnarsson, L.; Lewis, R. J. Expression and pharmacology of endogenous Ca_v channels in SH-SY5Y human neuroblastoma cells. *PLoS One* **2013**, *8*, e59293.
(24) Tikhonov, D. B.; Zhorov, B. S. Structural model for dihydropyridine binding to L-type calcium channels. *J. Biol. Chem.* **2009**, *284*, 19006−19017.
(25) (a) Wappl, E.; Mitterdorfer, J.; Glossmann, H.; Striessnig, J. Mechanism of dihydropyridine interaction with critical binding residues of L-type Ca^{2+} channel alpha 1 subunits. *J. Biol. Chem.* **2001**, *276*, 12730−12735. (b) Yamaguchi, S.; Okamura, Y.; Nagao, T.; Adachi-Akahane, S. Serine residue in the IIIS5-S6 linker of the L-type Ca^{2+} channel alpha 1C subunit is the critical determinant of the action of dihydropyridine Ca^{2+} channel agonists. *J. Biol. Chem.* **2000**, *275*, 41504−41511. (c) Schuster, A.; Lacinova, L.; Klugbauer, N.; Ito, H.; Birnbaumer, L.; Hofmann, F. The IVS6 segment of the L-type calcium channel is critical for the action of dihydropyridines and phenylalkylamines. *EMBO J.* **1996**, *15*, 2365−2370. (d) Peterson, B. Z.; Johnson, B. D.; Hockerman, G. H.; Acheson, M.; Scheuer, T.; Catterall, W. A. Analysis of the dihydropyridine receptor site of L-type calcium channels by alanine-scanning mutagenesis. *J. Biol. Chem.* **1997**, *272*, 18752−18758.
(26) (a) Zhorov, B. S.; Folkman, E. V.; Ananthanarayanan, V. S. Homology model of dihydropyridine receptor: implications for L-type Ca^{2+} channel modulation by agonists and antagonists. *Arch. Biochem. Biophys.* **2001**, *393*, 22−41. (b) Cosconati, S.; Marinelli, L.; Lavecchia, A.; Novellino, E. Characterizing the 1,4-dihydropyridines binding interactions in the L-type Ca^{2+} channel: model construction and docking calculations. *J. Med. Chem.* **2007**, *50*, 1504−1513.
(27) Goldmann, S.; Stoltefuß, J. 1,4-Dihydropyridines: Effects of Chirality and Conformation on Their Activity. In *Dihydropyridines*; Busse, W.-D., Garthoff, B., Seuter, F., Eds.; Springer: Berlin and Heidelberg, Germany, 1993; pp 24−35.
(28) (a) Marx, J. Alzheimer's disease. Fresh evidence points to an old suspect: calcium. *Science* **2007**, *318*, 384−385. (b) Green, K. N.; LaFerla, F. M. Linking calcium to Abeta and Alzheimer's disease. *Neuron* **2008**, *59*, 190−194.
(29) Rosini, M.; Simoni, E.; Bartolini, M.; Cavalli, A.; Ceccarini, L.; Pascu, N.; McClymont, D. W.; Tarozzi, A.; Bolognesi, M. L.; Minarini, A.; Tumiatti, V.; Andrisano, V.; Mellor, I. R.; Melchiorre, C. Inhibition of acetylcholinesterase, beta-amyloid aggregation, and NMDA receptors in Alzheimer's disease: a promising direction for the multi-target-directed ligands gold rush. *J. Med. Chem.* **2008**, *51*, 4381−4384.
(30) Maroto, R.; de la Fuente, M. T.; Artalejo, A. R.; Abad, F.; López, M. G.; García-Sancho, J.; García, A. G. Effects of Ca^{2+} channel antagonists on chromaffin cell death and cytosolic Ca^{2+} oscillations induced by veratridine. *Eur. J. Pharmacol.* **1994**, *270*, 331−339.
(31) (a) Marco-Contelles, J.; León, R.; de los Ríos, C.; Guglietta, A.; Terencio, J.; López, M. G.; García, A. G.; Villarroya, M. Novel multipotent tacrine−dihydropyridine hybrids with improved acetylcholinesterase inhibitory and neuroprotective activities as potential drugs for the treatment of Alzheimer's disease. *J. Med. Chem.* **2006**, *49*, 7607−7610. (b) Marco-Contelles, J.; León, R.; López, M. G.; García, A. G.; Villarroya, M. Synthesis and biological evaluation of new 4*H*-pyrano[2,3-*b*]quinoline derivatives that block acetylcholinesterase and cell calcium signals, and cause neuroprotection against calcium overload and free radicals. *Eur. J. Med. Chem.* **2006**, *41*, 1464−1469. (c) León, R.; Marco-Contelles, J. A step further towards multitarget drugs for Alzheimer and neuronal vascular diseases: targeting the cholinergic system, amyloid-beta aggregation and Ca^{2+} dyshomeostasis. *Curr. Med. Chem.* **2011**, *18*, 552−576.
(32) Khaliq, Z. M.; Bean, B. P. Pacemaking in dopaminergic ventral tegmental area neurons: depolarizing drive from background and voltage-dependent sodium conductances. *J. Neurosci.* **2010**, *30*, 7401−7413.
(33) Dryanovski, D. I.; Guzmán, J. N.; Xie, Z.; Galteri, D. J.; Volpicelli-Daley, L. A.; Lee, V. M.; Miller, R. J.; Schumacker, P. T.; Surmeier, D. J. Calcium entry and alpha-synuclein inclusions elevate dendritic mitochondrial oxidant stress in dopaminergic neurons. *J. Neurosci.* **2013**, *33*, 10154−10164.
(34) Egea, J.; Rosa, A. O.; Cuadrado, A.; García, A. G.; López, M. G. Nicotinic receptor activation by epibatidine induces heme oxygenase-1 and protects chromaffin cells against oxidative stress. *J. Neurochem.* **2007**, *102*, 1842−1852.
(35) Butterfield, D. A.; Drake, J.; Pocernich, C.; Castegna, A. Evidence of oxidative damage in Alzheimer's disease brain: central role for amyloid beta-peptide. *Trends Mol. Med.* **2001**, *7*, 548−554.
(36) Honda, K.; Smith, M. A.; Zhu, X.; Baus, D.; Merrick, W. C.; Tartakoff, A. M.; Hattier, T.; Harris, P. L.; Siedlak, S. L.; Fujioka, H.; Liu, Q.; Moreira, P. I.; Miller, F. P.; Nunomura, A.; Shimohama, S.; Perry, G. Ribosomal RNA in Alzheimer disease is oxidized by bound redox-active iron. *J. Biol. Chem.* **2005**, *280*, 20978−20986.
(37) (a) Romero, A.; Egea, J.; García, A. G.; López, M. G. Synergistic neuroprotective effect of combined low concentrations of galantamine and melatonin against oxidative stress in SH-SY5Y neuroblastoma cells. *J. Pineal Res.* **2010**, *49*, 141−148. (b) González-Muñoz, G. C.; Arce, M. P.; López, B.; Pérez, C.; Romero, A.; del Barrio, L.; Martín-de-Saavedra, M. D.; Egea, J.; León, R.; Villarroya, M.; López, M. G.; García, A. G.; Conde, S.; Rodríguez-Franco, M. I. *N*-Acylaminophenothiazines: neuroprotective agents displaying multifunctional activities for a potential treatment of Alzheimer's disease. *Eur. J. Med. Chem.* **2011**, *46*, 2224−2235.
(38) Parada, E.; Egea, J.; Romero, A.; del Barrio, L.; García, A. G.; López, M. G. Poststress treatment with PNU282987 can rescue SH-SY5Y cells undergoing apoptosis via alpha7 nicotinic receptors linked to a Jak2/Akt/HO-1 signaling pathway. *Free Radical Biol. Med.* **2010**, *49*, 1815−1821.
(39) Egea, J.; Rosa, A. O.; Sobrado, M.; Gandía, L.; López, M. G.; García, A. G. Neuroprotection afforded by nicotine against oxygen and glucose deprivation in hippocampal slices is lost in alpha7 nicotinic receptor knockout mice. *Neuroscience* **2007**, *145*, 866−872.
(40) Lau, A.; Tymianski, M. Glutamate receptors, neurotoxicity and neurodegeneration. *Pfluegers Arch.* **2010**, *460*, 525−542.
(41) Abramov, A. Y.; Duchen, M. R. Impaired mitochondrial bioenergetics determines glutamate-induced delayed calcium deregulation in neurons. *Biochim. Biophys. Acta* **2010**, *1800*, 297−304.
(42) Chen, H.; Yoshioka, H.; Kim, G. S.; Jung, J. E.; Okami, N.; Sakata, H.; Maier, C. M.; Narasimhan, P.; Goeders, C. E.; Chan, P. H. Oxidative stress in ischemic brain damage: mechanisms of cell death and potential molecular targets for neuroprotection. *Antioxid. Redox Signaling* **2011**, *14*, 1505−1517.
(43) Thomsen, R.; Christensen, M. H. MolDock: a new technique for high-accuracy molecular docking. *J. Med. Chem.* **2006**, *49*, 3315−3321.
(44) Gerber, P. R.; Muller, K. MAB, a generally applicable molecular force field for structure modelling in medicinal chemistry. *J. Comput.-Aided Mol. Des.* **1995**, *9*, 251−268.
(45) Denizot, F.; Lang, R. Rapid colorimetric assay for cell growth and survival. Modifications to the tetrazolium dye procedure giving improved sensitivity and reliability. *J. Immunol. Methods* **1986**, *89*, 271−277.
(46) Mulvany, M. J.; Halpern, W. Contractile properties of small arterial resistance vessels in spontaneously hypertensive and normotensive rats. *Circ. Res.* **1977**, *41*, 19−26.